Remote Sensing Image Segmentation Based on Probabilistic Fuzzy Local Information Clustering

Xiaoli Li[1], Longlong Zhao[1], Jinsong Chen[1]

[1]Center for Geospatial Information, Shenzhen Institute of Advanced Technology, Chinese Academy of Sciences, Shenzhen, China - xl.li2@siat.ac.cn, ll.zhao@siat.ac.cn, js.chen@siat.ac.cn

Keywords: Hidden Markov Random Field (HMRF), Fuzzy Local Information, Gaussian Distribution, Maximum Entropy Model, Remote Sensing Image Segmentation

Abstract

In this paper, a remote sensing image segmentation based on probabilistic fuzzy local information clustering algorithm is proposed. First, assuming that the spectral measure within the same ground object follows the same probability distribution. The dissimilarity between pixel and object is modeled by the negative logarithm of the Gaussian probability density function. It can improve the noise sensitive problem caused by the Euclidean distance which can only describe the data with isotropic distribution. Then, in order to consider the effect of local spatial constraint, on the one hand, the probability measure is used to modify the local fuzzy factor to establish the dissimilarity measure with spatial constraints. On the other hand, the hidden Markov random field is used to model the prior probability model of pixel membership. Next, the entropy regularization term of the objective function is built by combining the Kullback-Leibler(KL) maximum entropy model to further improve the robustness and noise resistance. The qualitative and quantitative analysis of simulated image and different types of real remote sensing images show that the proposed algorithm can effectively overcome the above problems and further improve the accuracy of image segmentation to over 95%.

1. Introduction

Image segmentation is the process of aggregating pixels according to certain rules to form several specific regions with similar features (Zhang et al., 2020). However, due to the complexity of the special imaging process, remote sensing image segmentation is full of uncertainty (Löw et al., 2015).

Fuzzy clustering is one of the effective tools to alleviate uncertainty in the image segmentation process (Memon et al., 2018). Fuzzy C-means (FCM) is the most representative algorithm. It extends the relationship between pixels and clustering from hard to soft by introducing fuzzy membership. FCM improved the impact of outliers. However, it still has some problems. Such as (1) It didn't consider the spatial neighborhood effect. The noise resistance is weak, (2) It used Euclidean distance to describe the dissimilarity between pixels and clusters. It can only describe data with spherical distribution characteristics.

To solve the first problem, Ahmed et al. (2002) proposed FCM_S. It introduced a regularization term modeled by the dissimilarity between neighborhood pixels and clustering. The noise resistance has been further improved. Next, Chen and Zhang (2004) proposed FCM_S1 and FCM_S2. They accelerated FCM_S with the help of mean filtering images. Krinidis and Chatzis (2010) proposed FLICM based on the idea of FCM_S. It introduced spatial distance weights on the basis of neighborhood pixel dissimilarity, which significantly improved noise resistance. Gong et al. (2012) proposed RFLICM. It proposed the local coefficient of variation model, and used it instead of spatial distance to characterize the strength of neighborhood interactions. It corrected the issue where the central pixel is an outlier.

To solve the second problem, Gustafson and Kessel (1978) proposed GK. It modeled the dissimilarity by mahalanobis distance, which extended the model's ability to characterize ellipsoidal distribution data. Next, Liu et al. focused on the covariance, and proposed FCM_M (Liu et al., 2007)、FCM_CM(Liu et al., 2009a) and FCM_SM (Liu et al., 2009b). Utilizing the feature representation ability of kernel functions, Chen and Zhang (2004) also proposed the robust kernelized versions KFCM_S, KFCM S1and KFCM S2. Then, Gong et al. (2013) proposed KWFLICM. It replaced the Euclidean distance in the fuzzy factor with a kernel function, which improved the robustness of the algorithm. Next, Memon and Lee (2018) proposed GKWFLICM. It is not limited to processing one-dimensional data and has achieved segmentation of raw data in multidimensional situations. However, the above methods are all based on distance measurement to characterize dissimilarity. They can not describe the random distribution characteristics of the data. Chatzis and Varvarigou (2008) proposed HMRF-FCM. It characterizes dissimilarity based on Gaussian distribution and neighborhood constraint based on Markov random field, which greatly improved the image segmentation effect. However, it did not consider the situation where neighboring pixels are noisy.

Therefore, a probabilistic fuzzy local information clustering algorithm for image segmentation is proposed in this paper. On the basis of the local coefficient of variation, it corrected the dissimilarity measure with a Gaussian distribution probability density function. Then, the probability fuzzy local information is obtained to further accurately characterize the features between pixels and clusters. Besides, a prior probability model is established based on the hidden Markov random field model to further consider the neighborhood effect. Finally, combining the above model, the clustering objective function is built based on the Kullback Leibler (KL) maximum entropy theory.

This contribution has been peer-reviewed. The double-blind peer-review was conducted on the basis of the full paper.
https://doi.org/10.5194/isprs-annals-X-4-2024-211-2024 | © Author(s) 2024. CC BY 4.0 License.

2. Methodology

2.1 Segmentation objective function

Given a remote sensing image $\boldsymbol{X} = \{\boldsymbol{x}_i : i = 1, \ldots, n\}$. Where i is the index of pixels, n is the total number of pixels, $\boldsymbol{x}_i$ is the spectral feature vector of pixel i. Assuming there are c clusters in the image. The membership degree of pixels between clusters is $\boldsymbol{U}=[u_{ij}]_{n\times c}$, where j is the index of clusters. $\boldsymbol{U}$ needs to meet the constraints, $0 \le u_{ij} \le 1$, $\sum_{j=1}^{c} u_{ij} = 1$. $\boldsymbol{L}=\{l_i, i = 1,...,n\}$ is ac label set, which is used to represent the labels of the clusters to which pixels belong.

Based on the above information, the segmentation objective function model in this paper is modeled as,

$$J = \sum_{i=1}^{n}\sum_{j=1}^{c} u_{ij}\left(d_{ij} + G_{ij}\right) + \lambda \sum_{i=1}^{n}\sum_{j=1}^{c} u_{ij} \log\left(\frac{u_{ij}}{\pi_{ij}}\right) \tag{1}$$

Where the second term is the KL entropy regularization term. λ is the coefficient of KL entropy regularization term, which is used to characterize the fuzzy degree of the algorithm. The larger the λ is, the greater the pixel difference within homogeneous regions in segmentation results. d_{ij} is the dissimilarity between pixel i and cluster j. G_{ij} is fuzzy local factor. π_{ij} is the prior probability that pixel i belongs to cluster j.

To describe the random distribution of clusters, d_{ij} is modeled by the negative logarithm of the probability density function of Gaussian distribution,

$$\begin{aligned} d_{ij} &= -\log\, p(\boldsymbol{x}_i \mid l_i = j, \boldsymbol{\mu}_j, \boldsymbol{\Sigma}_j) \\ &= -\log\left\{\frac{1}{\sqrt{(2\pi)^w \mid \boldsymbol{\Sigma}_j \mid}} \exp\left[-\frac{1}{2}(\boldsymbol{x}_i - \boldsymbol{\mu}_j)\boldsymbol{\Sigma}_j^{-1}(\boldsymbol{x}_i - \boldsymbol{\mu}_j)^T\right]\right\} \end{aligned} \tag{2}$$

Where w is dimension of bands. $\boldsymbol{\mu}_j$ and $\boldsymbol{\Sigma}_j$ are the mean and variance of the Gaussian distribution followed by cluster j, respectively. When $w = 1$, the Gaussian distribution in Equation (2) degenerates into a normal distribution.

Based on Equation (2), combining the local coefficient of variation, the fuzzy local factor is modeled as,

$$G_{ij} = \begin{cases} \sum_{i'\in\partial_i} \dfrac{\left(1-u_{i'j}\right)d_{i'j}}{2 + \min\left[\left(\dfrac{C_{i'}}{C_i}\right)^2, \left(\dfrac{C_i}{C_{i'}}\right)^2\right]}, & C_{i'} \ge \overline{C_i} \\ \sum_{i'\in\partial_i} \dfrac{\left(1-u_{i'j}\right)d_{i'j}}{2 - \min\left[\left(\dfrac{C_{i'}}{C_i}\right)^2, \left(\dfrac{C_i}{C_{i'}}\right)^2\right]}, & C_{i'} < \overline{C_i} \end{cases} \tag{3}$$

Where $\partial = \{\partial_i : i = 1, ...,n\}$ is the neighborhood system, $i' \in \partial_i$, $i' \ne i$. C_i is the local coefficient of variation of pixel i. It is used to represent the difference in spectral measurements between pixel i and its neighboring pixels.

$$\begin{aligned} C_i^1 &= \frac{\sigma^2(x_i)}{\overline{x_i}^2} \\ C_i^2 &= \frac{1}{\overline{\boldsymbol{x}_i}\boldsymbol{\Sigma}(x_i)^{-1}\overline{\boldsymbol{x}_i}^{\mathrm{T}}} \end{aligned} \tag{4}$$

Where C_i^1 and C_i^2 correspond to the local coefficient of variation for w=1 and w>1, respectively. $\overline{x_i}$ is the mean spectral measure of neighboring pixels centered on pixel i, $\sigma^2(x_i)$ and $\Sigma(x_i)$ are the variance and covariance.

To further consider the effect of neighboring pixels, the prior probability π_{ij} is modeled based on the theory of hidden Markov random fields,

$$\pi_{ij} = p(l_i = j \mid l_{i'}, i' \in \partial_i) = \frac{\exp\left(\beta \sum_{i'\in\partial_i} \delta(l_i = j, l_{i'})\right)}{\sum_{k=1}^{c} \exp\left(\beta \sum_{i'\in\partial_i} \delta(l_i = k, l_{i'})\right)} \tag{5}$$

Where k is also the index of clusters, β is the strength of neighborhood interaction, $\delta(a, b)$ is energy function, if and only if $a = b$, $\delta = 1$, otherwise $\delta = 0$.

2.2 Parameter solving

Due to the objective function J clearly expressing the mean $\boldsymbol{\mu}_j$ and covariance $\boldsymbol{\Sigma}_j$. By directly taking the derivative of the objective function and making the derivative 0, we obtain,

$$\boldsymbol{\mu}_j = \frac{\sum_{i=1}^{n} u_{ij}\boldsymbol{x}_i}{\sum_{i=1}^{n} u_{ij}} \tag{6}$$

$$\boldsymbol{\Sigma}_j = \frac{\sum_{i=1}^{n} u_{ij}(\boldsymbol{x}_i - \boldsymbol{\mu}_j)^T(\boldsymbol{x}_i - \boldsymbol{\mu}_j)}{\sum_{i=1}^{n} u_{ij}} \tag{7}$$

Due to the constraint of membership degree $\boldsymbol{U}$, it is necessary to construct a Lagrangian function and set its derivative to 0. We obtain,

$$u_{ij} = \frac{\pi_{ij} \exp\left(-\dfrac{d_{ij} + G_{ij}}{\lambda}\right)}{\sum_{k=1}^{c} \pi_{ik} \exp\left(-\dfrac{d_{ik} + G_{ik}}{\lambda}\right)} \tag{8}$$

The optimal model parameters are obtained through iteration. Furthermore, the optimal image segmentation result is also obtained. The final label l_i^* to which the pixel belongs is obtained from the defuzzification,

$$l_i^* = \arg\max_{j=1}^{c}\{u_{ij}^*\} \tag{9}$$

Where u_{ij}^* is the optimal fuzzy membership.

2.3 Summary of the proposed algorithm

The process of the proposed algorithm can be summarized as follows,

This contribution has been peer-reviewed. The double-blind peer-review was conducted on the basis of the full paper.
https://doi.org/10.5194/isprs-annals-X-4-2024-211-2024 | © Author(s) 2024. CC BY 4.0 License.

S1: Set constants. Such as the number of clusters c, KL regularization coefficient λ, Neighborhood influence strength β, iteration stop condition parameter ε;

S2: Initialization. Iteration indicator $t = 0$, randomly generate initial membership matrix $\boldsymbol{U}^{(0)}$, and obtain initial label $\boldsymbol{L}^{(0)}$ through defuzzification;

S3: Calculate the mean $\boldsymbol{\mu}_j^{(t)}$ and $\boldsymbol{\Sigma}_j^{(t)}$ according to Equations (6) and (7), and calculate the dissimilarity measure $d_{ij}^{(t)}$ according to Equation (2);

S4: Calculate the local coefficient of variation $C_i^{(t)}$ according to Equation (4), and obtain the fuzzy local factor $G_{ij}^{(t)}$ according to Equation (3);

S5: Calculate the prior probability $\pi_{ij}^{(t)}$ according to Equation (5);

S6: Calculate the membership degree $\boldsymbol{U}^{(t)}$ according to Equation (8);

S7: Calculate the objective function $J^{(t)}$ according to Equation (1);

S8: If $\max|J^{(t)} - J^{(t-1)}| < \varepsilon$, exit the loop, otherwise let $t = t+1$ and return to S3 to continue iterating.

3. Experiments

In order to verify the effectiveness of the proposed algorithm, FCM, FCM_S, FLICM, RFLICM, and HMRF-FCM algorithms were used as comparative algorithms to perform segmentation experiments on simulated and real remote sensing images, and the segmentation results were qualitatively and quantitatively analyzed.

3.1 Simulated images

In order to simulate the random distribution characteristics of spectral measurements of ground objects, a simulated image that follows Gaussian distribution characteristics is randomly generated based on the template image, where I-IV represents different homogeneous regions, as shown in Figure 1. Their distribution parameters are shown in Table 1. To highlight the effectiveness of the proposed algorithm, regions I and III have the same mean, and regions III and IV have the same standard deviation.

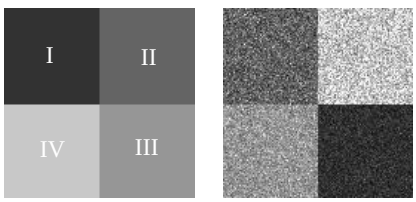

(a) (b)

Figure 1. (a) Template, (b) Simulated image.

Parameters	Homogeneous regions			
	I	II	III	IV
Mean	10	20	10	30
Standard deviation	10	10	5	5

Table 1. Gaussian distribution parameters.

Figure 2 shows the simulated image segmentation results, where Figures 2 (a1) - (f1) show the segmentation results of FCM, FCM_S, FLICM, RFLICM, HMRF-FCM, and the proposed algorithm, respectively. Figures 2 (a2) - (f2) show the overlapping images of the corresponding segmentation results. As shown in Figure 2, the FCM algorithm has the worst noise resistance, with salt and pepper noise almost covering the entire region in the segmentation results; The FCM_S algorithm introduces spatial neighborhood constraints, which reduces the degree of salt and pepper noise, but the segmentation effect is still poor. The FLICM algorithm constructs fuzzy local factors by introducing neighborhood pixel spatial distance and fuzzy membership degree, greatly reducing the impact of noise and outliers. However, for Region II with high spectral variance, its noise resistance is significantly lower than Region III with low variance. In addition, there is also a tendency for confusion in segmentation at the boundaries of homogeneous regions; RFLICM introduces local variation coefficients to correct fuzzy local factors on the basis of FLICM, further improving the segmentation effect, as shown in region II in Figure 2 (d1) and (d2). HMRF-FCM describes the random distribution of pixels in homogeneous regions based on Gaussian distribution, and constructs a KL entropy regularization model in combination with hidden Markov random field theory. It effectively solved the problem of distance measurement being difficult to characterize randomly distributed data, greatly suppressing the influence of noise, but there is still a certain degree of misclassification phenomenon, as shown in Figure 2 (e1) and (e2). This paper combines Gaussian distribution and its modified fuzzy local factors to construct a dissimilarity measure with spatial constraints. On the one hand, it effectively characterizes the random distribution of the data, and on the other hand, it strengthens the spatial neighborhood pixel constraint, effectively improving the segmentation effect. There is no misclassification noise in each homogeneous region, as shown in Figure 2 (f1) and (f2).

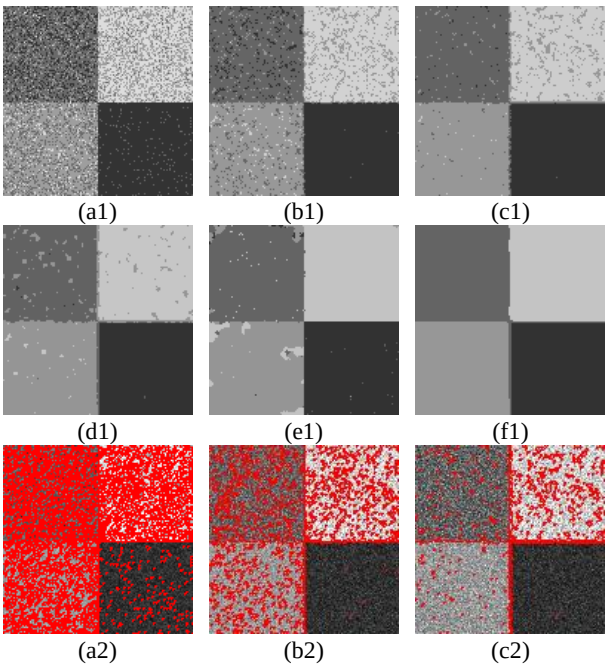

(a1) (b1) (c1)

(d1) (e1) (f1)

(a2) (b2) (c2)

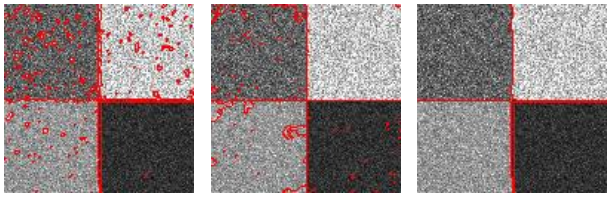

(d2) (e2) (f2)

Figure 2. Segmentation results of simulated images. (a1) - (f1) show the segmentation results of FCM, FCM_S, FLICM, RFLICM, HMRF-FCM, and the proposed algorithm, respectively, (a2) - (f2) show the overlapping images of the corresponding segmentation results.

In order to quantitatively evaluate the effectiveness of segmentation results, a confusion matrix was generated based on template images for the segmentation results in Figure 2, and user accuracy, product accuracy, overall accuracy, and Kappa values were calculated and listed in Table 2. According to Table 2, FCM algorithm has the lowest accuracy, with a user accuracy of only 49.93% in Region II, and overall accuracy and Kappa value of only 66.96% and 0.56%. FCM_S algorithm has greatly improved compared to FCM, but it is still less than 90%. FLICM algorithm can reach 93.83%, and the Kappa value exceeds 0.9. RFLICM has further improved by about 2 percentage points on the basis of FLICM algorithm. HMRF-FCM has the highest accuracy in the comparison algorithm, reaching 96.81%, and the user and product accuracy in each region are both above 90%, but it is still not as good as the proposed algorithm. The proposed algorithm has overall accuracy of 98.8% and Kappa value of 0.98. The effectiveness of the proposed algorithm was accurately validated through quantitative analysis.

Algorithms	Accuracy (%)	Homogeneous regions			
		I	II	III	IV
FCM	User	59.01	89.03	77.56	52.11
	Product	60.63	49.93	96.53	61.51
	Overall = 66.96		Kappa = 0.56		
FCM_S	User	89.44	95.34	91.86	77.04
	Product	86.15	80.24	99.03	86.53
	Overall = 87.92		Kappa = 0.84		
FLICM	User	95.41	99.33	99.02	83.82
	Product	95.96	84.93	97.50	97.15
	Overall = 93.83		Kappa = 0.92		
RFLICM	User	95.93	98.42	99.80	87.62
	Product	92.84	94.33	96.83	96.90
	Overall = 95.20		Kappa = 0.94		
HMRF-FCM	User	98.68	93.24	99.26	96.41
	Product	95.36	99.74	99.50	92.58
	Overall = 96.81		Kappa =0.96		
Proposed	User	95.82	99.62	100	100
	Product	99.62	99.95	96.88	98.69
	Overall = 98.80		Kappa = 0.98		

Table 2. Quantitative evaluation of the simulated image.

In order to further verify the ability of probability measures in the proposed algorithm to characterize the distribution characteristics of spectral measures in homogeneous regions, a Gaussian distribution function curve is drawn as shown in Figure 3. Figures 3 (a) - (d) represent regions I-IV, black represents the true distribution function curve, blue represents the Gaussian distribution function in the HMRF-FCM model, and red represents the Gaussian distribution function of the proposed algorithm. As shown in Figure 3, the proposed algorithm function curve is closer to the true curve, especially for regions III and IV with small standard deviations, which almost overlap, as shown in Figures 3 (c) and (d). Figure 3 further effectively verifies the ability of the proposed algorithm to characterize randomly distributed data.

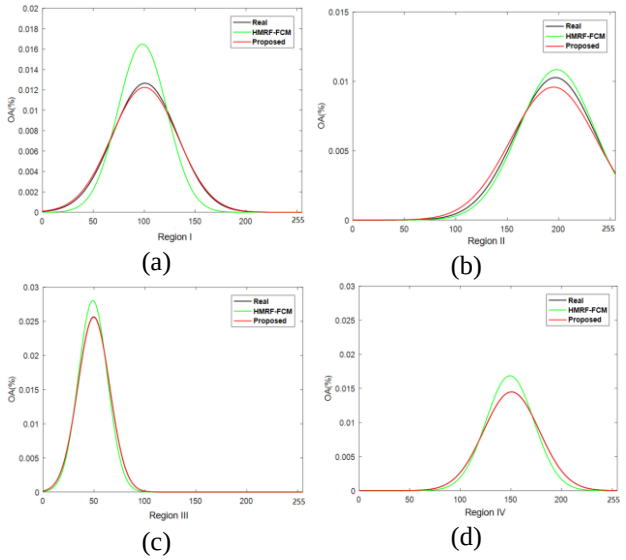

(a) (b) (c) (d)

Figure 3. Gaussian distribution function fitting, (a) - (d) represent regions I-IV.

3.2 Real remote sensing images

In order to verify the applicability of the proposed algorithm to different types of remote sensing images, multispectral remote sensing images and SAR images were selected for segmentation performance testing, as shown in Figure 4. Figures 4 (a1) - (c1) represent multispectral remote sensing images and SAR images captured from Spot-5, IKONOS, and RADARSAT-II, respectively. Figures 4 (a2) - (c2) represent the corresponding template images.

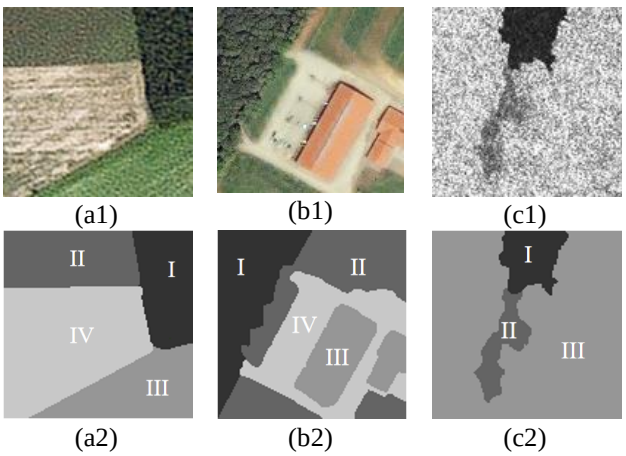

(a1) (b1) (c1)

(a2) (b2) (c2)

Figure 4. Real remote sensing images. (a1) Spot-5, (b1) IKONOS, (c1) RADARSAT-II. (a2) - (c2) the corresponding template images.

Figure 5 shows the segmentation results of real remote sensing images. Each row represents different remote sensing images. The different columns are FCM, FCM_S, FLICM, RFLICM, HMRF-FCM, and the segmentation results proposed by the algorithm. The overlapping images of the corresponding segmentation results are shown in Figure 6. From Figures 5 and 6, it can be seen that the FCM algorithm and FCM_S algorithm

This contribution has been peer-reviewed. The double-blind peer-review was conducted on the basis of the full paper.
https://doi.org/10.5194/isprs-annals-X-4-2024-211-2024 | © Author(s) 2024. CC BY 4.0 License.

have poor noise resistance, especially difficult to overcome the influence of speckle noise in SAR images, as shown in Figures 5, 6 (a1) and (b1) - (a3) and (b3). The FLICM algorithm and RFLICM algorithm introduce neighborhood pixel effects, which can effectively overcome the influence of speckle noise, but cannot effectively segment object with large area heterogeneity (region IV in Figure 4), as shown in Figures 5, 6 (c1) and (d1). The HMRF-FCM algorithm replaces the Euclidean distance in the above method with a Gaussian distribution, and introduces spatial constraints in combination with the Markov random field model, greatly overcoming the influence of noise and outliers. It can achieve effective segmentation of different types of images, but there is still some segmentation noise, as shown in Figures 5, 6 (e1) - (e3). According to Figures 5, 6 (f1) - (f3), it can be seen that the proposed algorithm can further overcome the impact of different types of noise such as large area heterogeneity and speckle on segmentation results. There is almost no salt and pepper noise in homogeneous regions, and the boundaries of homogeneous regions are relatively smooth. The segmentation effect has been greatly improved.

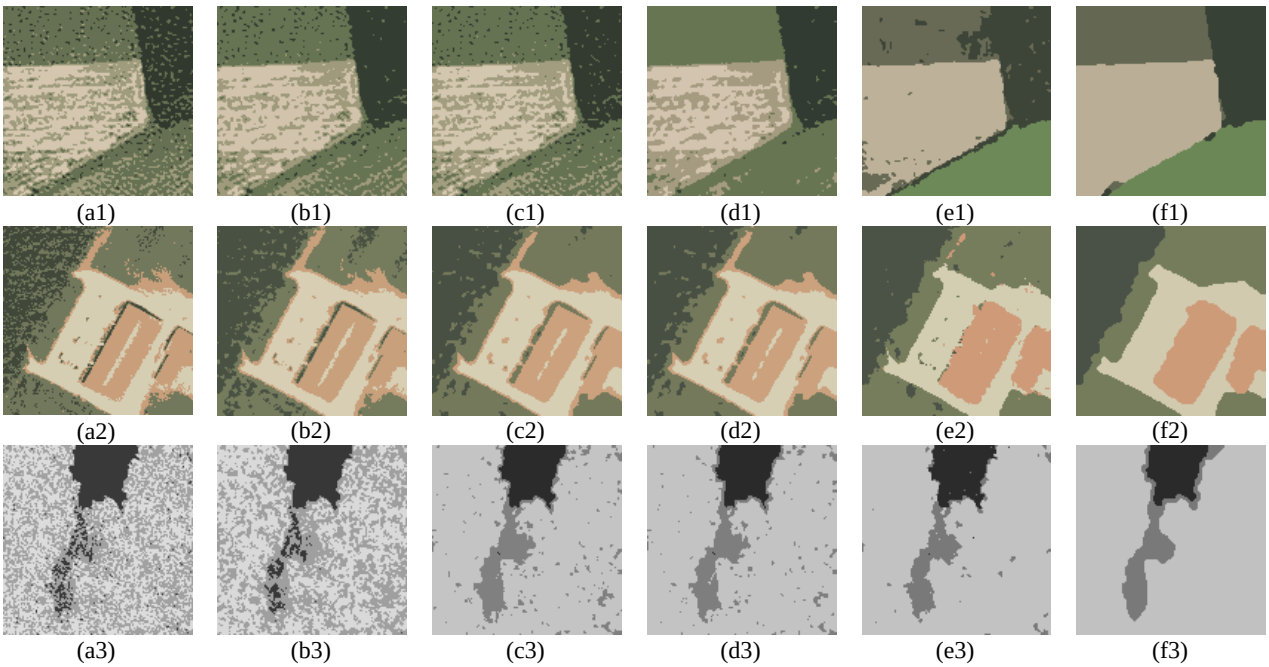

Figure 5. Segmentation results of real remote sensing images. (a1)-(a3) FCM, (b1)-(b3) FCM_S, (c1)-(c3) FLICM, (d1)-(d3) RFLICM, (e1)-(e3) HMRF-FCM, (f1)-(f3) The proposed algorithm.

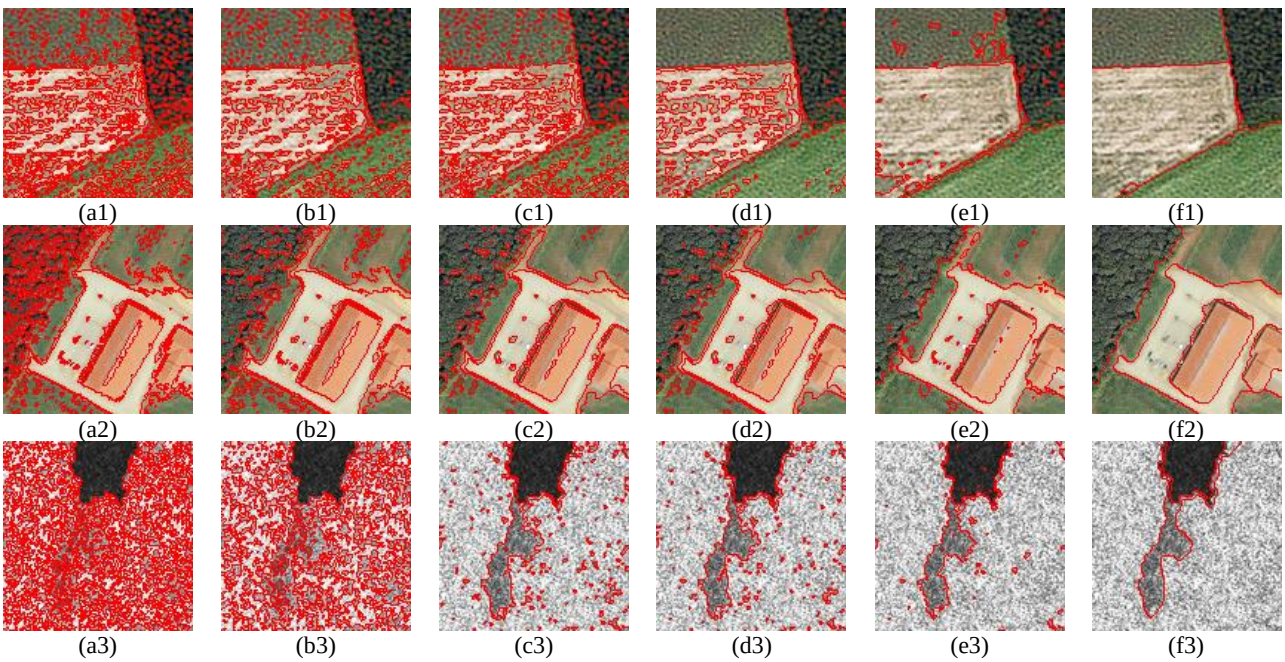

Figure 6. The overlapping images of real remote sensing images. (a1)-(a3) FCM, (b1)-(b3) FCM_S, (c1)-(c3) FLICM, (d1)-(d3) RFLICM, (e1)-(e3) HMRF-FCM, (f1)-(f3) The proposed algorithm.

This contribution has been peer-reviewed. The double-blind peer-review was conducted on the basis of the full paper.
https://doi.org/10.5194/isprs-annals-X-4-2024-211-2024 | © Author(s) 2024. CC BY 4.0 License.

Table 3 shows the quantitative evaluation results of real remote sensing image segmentation. From Table 3, it can be seen that Figure 4 (a1) is affected by the large-scale heterogeneous noise in region IV, and the segmentation accuracy of each algorithm is relatively low. HMRF-FCM can improve the accuracy from about 60% to 90%. The proposed algorithm corrects the fuzzy local factor based on probability measurement, combined with the hidden Markov random field model, and introduces spatial constraints from different perspectives, achieving a segmentation accuracy of 98.36%. The region I in Figure 4 (a2) has a large variance, which is the main factor affecting segmentation accuracy. With the strengthening of spatial constraints, the accuracy gradually increases. Figure 4 (a3) is affected by the inherent speckle noise in SAR images, and the accuracy of FCM and FCM_S algorithms is only 60%. FLICM, RFLICM, and HMRF-FCM can improve their segmentation accuracy to over 90% through spatial constraints. The proposed algorithm has a higher accuracy, reaching 96.56%. By quantitatively analyzing the segmentation accuracy of different types of remote sensing images, the feasibility and effectiveness of the proposed algorithm in real remote sensing image segmentation have been further verified.

Images	Algorithms					
	FCM	FCM_S	FLICM	RFLICM	HMRF-FCM	Proposed
Figure 4(a1)	58.90	62.59	59.20	58.62	92.09	98.36
Figure 4(b1)	78.77	81.34	85.35	85.39	94.26	95.27
Figure 4(c1)	56.65	60.67	93.62	94.30	95.60	96.56

Table 3. Quantitative evaluation of real remote sensing images. (Overall accuracy: %)

4. Conclusion

In this paper, a remote sensing image segmentation algorithm based on probabilistic fuzzy local information clustering is proposed. The dissimilarity is modeled based on probability measures to describe the random distribution characteristics of data. The modified fuzzy local factor is modeled by the local coefficient of variation and probability measures, which can more accurately describe the local features. In addition, combining the hidden Markov random field theory to model the prior probability and establishing the KL maximum entropy regularization term, it can further strengthen the spatial constraint effect. Through qualitative and quantitative analysis of simulated images and different types of real remote sensing images, the proposed algorithm's noise resistance and robustness have been effectively verified. In future research, it is planned to extend this algorithm to the object-oriented level to expand its application in high-resolution remote sensing image processing on a large regional scale.

Acknowledgements

This research was funded by the Excellent Youth Innovation Foundation of the Shenzhen Institutes of Advanced Technology (SIAT) of the Chinese Academy of Science (CAS), grant number E3G044, the National Natural Science Foundation of China, grant number 42001286, the Key Project of the Fundamental Research Foundation of Shenzhen Science and Technology Innovation Committee, Grants number JCYJ20200109115637548 and JCYJ20220818101617038, and the Scientific Research Project of Ecology Environment Bureau of Shenzhen Municipality, Grant number SZDL2023001387.

References

Ahmed, M.N., Yamany, S.M., Mohamed, N., Farag, A.A., Moriarty, T., 2002. A modified fuzzy c-means algorithm for bias field estimation and segmentation of MRI data. *IEEE Transactions on Medical Imaging*, 21(3), 193-199.

Chatzis, S.P., Varvarigou, T.A., 2008. A fuzzy clustering approach toward hidden Markov random field models for enhanced spatially constrained image segmentation. *IEEE Transactions on Fuzzy Systems*, 16(5), 1351-1361.

Chen, S., Zhang, D., 2004. Robust image segmentation using FCM with spatial constraints based on new kernel-induced distance measure. *IEEE Transactions on Cybernetics Systems, Man and Cybernetics*, 34(4), 1907-1916.

Gong, M., Zhou, Z., Ma, J., 2012. Change detection in synthetic aperture radar images based on image fusion and fuzzy clustering. *IEEE Transactions on Image Processing*, 21(4), 2141-2151.

Gong, M., Liang, Y., Shi, j., Ma, W., Ma, J., 2013. Fuzzy C-means clustering with local information and kernel metric for image segmentation. *IEEE Transactions on Image Processing*, 22 (2), 573-584.

Gustafson, D.E., Kessel, W.C., 1978. Fuzzy clustering with a fuzzy covariance matrix. *In the 1978 IEEE Conference on Decision and Control including the 17th Symposium on Adaptive Processes*, San Diego, CA, USA, pp. 761-766.

Krinidis, S., Chatzis, V., 2010. A robust fuzzy local information c-means clustering algorithm. *IEEE Transactions on Image Processing*, 19(5), 1328-1337.

Löw, F., Knöfel, P., Conrad, C., 2015. Analysis of uncertainty in multi-temporal object-based classification. *ISPRS Journal of Photogrammetry and Remote Sensing*, 105, 91-106.

Liu, H.C., Yih, J.M., Liu, S.W., 2007. Fuzzy c-mean algorithm based on Mahalanobis distances and better initial values. In *the 10th Joint Conference and 12th International Conference on Fuzzy Theory & Technology*, UK: World Scientific Publishing, pp. 1398-1404.

Liu, H.C., Yih, J.M., Lin, W.C., Wu, D.B., 2009a. Fuzzy c-means algorithm based on common Mahalanobis distances. *Journal of Multiple Valued Logic and Soft Computing*, 15(5), 581-595.

Liu, H.C., Jeng, B.C., Yih, J.M., Yu, Y.K., 2009b. Fuzzy c-means algorithm based on standard Mahalanobis distances. In *the 2009 International Symposium on Information Processing*, China: 2009 Academy Publisher, pp. 422-427.

Memon, K.H., Lee, D.H., 2018. Generalised kernel weighted fuzzy c-means clustering algorithm with local information. *Fuzzy and Sets*, 340, 91-108.

Zhang, X., Xiao, P., Feng, X., 2020. Object-specific optimization of hierarchical multiscale segmentations for highspatial resolution remote sensing images. *ISPRS Journal of Photogrammetry and Remote Sensing*, 159, 308-321.